Measured energy - momentum densities of the valence band of aluminium

1997 J. Phys.: Condens. Matter 9 1931

(http://iopscience.iop.org/0953-8984/9/9/008)

J. Phys.: Condens. Matter **9** (1997) 1931–1950. Printed in the UK PII: S0953-8984(97)77438-1

Measured energy–momentum densities of the valence band of aluminium

S A Canney, M Vos†, A S Kheifets, N Clisby, I E McCarthy and E Weigold†

Electronic Structure of Materials Centre, Flinders University of South Australia, GPO Box 2100, Adelaide, SA 5001, Australia

Received 29 August 1996

Abstract. The energy-resolved momentum densities of the valence band of a thin polycrystalline aluminium film have been measured using electron momentum spectroscopy (EMS). The spectrometer used for these measurements has estimated energy and momentum resolutions of 0.9 eV and 0.10 atomic units respectively. The valence band of aluminium was clearly resolved, resembling very closely that of a free-electron parabola. The measurement has been compared to linear muffin-tin orbital (LMTO) calculations for spherically averaged crystalline aluminium. A comparison has also been made between the experiment and Monte Carlo simulations which take into account additional elastic and inelastic scattering events not considered in the LMTO calculations. The final agreement obtained between the measurement and theory for the dispersion and relative intensities of the aluminium valence band is excellent when lifetime broadening of the band is allowed for.

1. Introduction

Electron momentum spectroscopy (EMS) (also called (e, 2e) spectroscopy) is an experimental technique which allows the direct determination of the momentum densities of the electrons as a function of binding energy. The conservation of energy and that of momentum form the basis of this technique. It has proved to be a very successful technique for studying the wave-functions of atoms and molecules. These gas-phase experiments are now very well established; see for example the reviews by McCarthy and Weigold [1, 2]. An excellent example illustrating the agreement obtainable between the experiment and calculation in atomic and molecular studies is the study by Lohmann and Weigold [3] on the 1s wave-function of atomic hydrogen.

The notation (e, 2e) refers to a process in which a high-energy incident electron (energy E_0, momentum $\boldsymbol{p}_0$) knocks out a target electron, with subsequent detection of both outgoing electrons. These outgoing electrons are detected in coincidence to ensure that they originated from the same scattering event. After detection of the (e, 2e) event, the energies (E_f and E_s) and momenta ($\boldsymbol{p}_f$ and $\boldsymbol{p}_s$) of both outgoing electrons are determined. For convenience we have respectively labelled the outgoing electrons with the subscript *f* for the faster one and *s* for the slower one. The binding energy ε and momentum $\boldsymbol{q}$ of the target electron

† Present address: Research School of Physical Sciences and Engineering, Institute of Advanced Studies, ANU, Canberra, ACT 0200, Australia

0953-8984/97/091931+20$19.50

before the collision are given by the following conservation laws:

$$\varepsilon = E_0 - E_s - E_f. \tag{1}$$

$$\boldsymbol{q} = \boldsymbol{p}_s + \boldsymbol{p}_f - \boldsymbol{p}_0. \tag{2}$$

Hence the (e, 2e) technique is kinematically complete—that is, all of the kinematic information regarding the scattering event is obtained. During an (e, 2e) experiment the energy-resolved electron momentum density is measured. In the independent-particle approximation this is equal to the absolute square of the momentum-space wave-function ($|\phi(\varepsilon, \boldsymbol{q})|^2$)—hence the common reference to 'wave-function mapping'. The (e, 2e) technique therefore directly determines the electron distribution in momentum space in the system of interest, and is consequently more commonly referred to as electron momentum spectroscopy.

The application of EMS to solids has been restricted in comparison with that to gas-phase targets, largely due to the complications which arise from the higher atomic densities. These electron scattering experiments require much higher energies of the incoming and outgoing electrons to avoid additional scattering events other than the (e, 2e) event itself. For solids one is also required to use a transmission mode in order to determine ($|\phi(\varepsilon, \boldsymbol{q})|^2$) for all $\boldsymbol{q}$. This requirement means that the solid-state targets must be very thin membranes ($\leqslant$200 Å) to enable the electrons to emerge from the back of the film. Even with thin samples and at high energies, multiple scattering occurs. Multiple scattering gives (e, 2e) events with changed energies (due primarily to inelastic events such as plasmon excitation) and momenta (in large part due to elastic events) affecting the direct relation between the measured intensities and the calculated wave-function. This results in a degradation in contrast in the experimentally determined energy-resolved momentum densities. Multiple scattering also causes increased random background events and hence reduces the ratio of the coincidence signal to the random background signal. As a result of this, longer collection times are required to obtain the desired statistical accuracy of the data.

In order to obtain detailed information on the electronic structure of the target, high coincidence count rates and good energy and momentum resolutions are required. The early (e, 2e) experiments on solids [4–6] were unable to resolve any valence band structure because of poor energy resolution. It was not until the experiments of Ritter *et al* [7], where the energy resolution had improved to 6 eV, that structure in the valence bands could be resolved. However, these experiments were still very restricted by coincidence rates and energy and momentum resolutions. The (e, 2e) spectrometer used for our measurements was described in detail by Storer *et al* [8]. The major difficulties involved in the measurements on solids have been successfully overcome by utilizing multi-parameter detection techniques and an improvement to the energy resolution with an electron monochromator; see Canney *et al* [9]. The improvements in design and technology incorporated into this spectrometer make (e, 2e) of solids a very powerful experimental technique.

Angle-resolved photoelectron spectroscopy (ARPES) is another experimental technique which is able to map the dispersion relation in crystals; see for example Courths and Hufner [10]. Although limited to single-crystal surfaces, this technique has been very successful and widely used. However, the theoretical understanding of the intensities of the observed peaks is far from complete. This is the case because the interaction process is very complicated, involving a many-body problem in the initial and final states. Also the outgoing photoelectrons have a very small escape depth due to the low kinetic energies of the electrons involved. The implications of this are that one has to overcome strongly damped states and also the contribution of the surface states must then be considered. These complications make it very difficult to describe accurately the interaction of photons

with the electrons in the solid. Hence it is not straightforward to measure the momentum densities of the electrons using ARPES. A technique that does enable the measurement of momentum densities is Compton scattering (see for example Cooper [11] for a review). This technique probes the target electrons with high-energy photons. A measurement of the total momentum density of all target electrons integrated over a plane perpendicular to the scattering vector is obtained. Thus only a projection of the momentum is obtained; information about the energy is not resolved.

In comparison, EMS measurements on any solid not only allow the direct observation of energy–momentum dispersion relations, but they also provide information on the densities of the electrons in the given band. Up until now these data on the behaviour of electrons in solids (energy, momentum and intensity) have not been measured entirely for any of the experiments reported. Total agreement has not been identified between the experimental results and theoretical calculations. This paper presents a further step down the path towards a fully quantitative spectroscopy of valence bands.

(e, 2e) spectroscopy was used to measure the collective properties of a degenerate electron gas in aluminium by Persiantseva *et al* [6]. This measurement was substantially restricted by energy resolution (16 eV). Williams and Hayes [12] also used (e, 2e) spectroscopy to measure the structure of aluminium/aluminium oxide. Their experiment had an energy resolution of 1.5 eV and a momentum resolution of 0.45 au. However, this experiment was unable to reveal the free-electron parabolic band because of the quantity of oxygen adsorbed on the surface. For some time now the valence band structure of aluminium has been accepted as free-electron-like and hence has not been extensively studied.

In this paper we report on the valence band measurements of the energy–momentum density of metallic aluminium. These experimental results are compared to linear muffin-tin orbital (LMTO) calculations for the band structure of aluminium. The measurements are also compared to Monte Carlo simulations of the experimental process which account for additional electron collisions other than the (e, 2e) collision, i.e. multiple-scattering events not included in the LMTO calculations. Aluminium, being a nearly free-electron metal, has a band structure that is well understood. Hence the agreement reached between the experiment and theory provides an excellent insight into our current understanding for (e, 2e) of solids.

2. Experimental details

The present (e, 2e) spectrometer was designed for the study of solid targets with the aim of producing high coincidence count rates, good energy resolution and good momentum resolution. To achieve these criteria an (e, 2e) coincidence spectrometer was built that utilizes asymmetric, non-coplanar kinematics. A schematic representation detailing these points is shown in figure 1. For more details on this spectrometer see Storer *et al* [8]. The energy resolution of the spectrometer has recently been improved with the incorporation of an electron monochromator for production of the incident electron beam [9]. The measured energy and momentum resolutions of the coincidence spectrometer are 0.9 eV and 0.15 au respectively.

During a typical (e, 2e) experiment on valence electrons with this spectrometer the incident energy is 20 keV, with the energy of the fast electron nominally 18.8 keV and the energy of the slow electron about 1.2 keV. Constant polar angles of 14° and 76° are used for the detection of the fast and slow electrons respectively. With this geometry the measured momentum $\boldsymbol{q}$ for a coplanar event, i.e. one with all three momentum vectors in the same plane, is zero. A range of azimuthal (out-of-plane) angles are measured simultaneously by

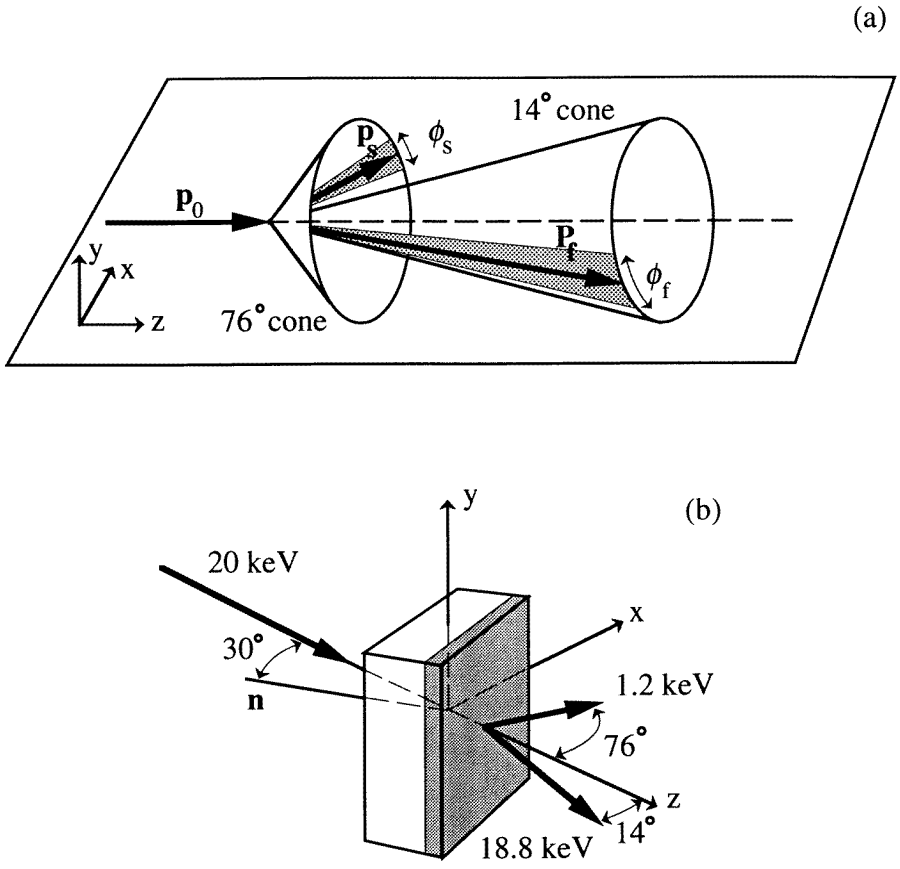

Figure 1. A schematic representation of the geometry of the (e, 2e) experiments. In (a) we show the range of angles measured. In (b) the sample orientation with respect to all three electron beams is shown. Most structural information is obtained from the shaded area of the sample since the slow electron has the smallest mean free path.

both detectors. The fast electron is detected in a hemispherical analyser whilst a toroidal analyser detects the slow electron. Each electron analyser has a two-dimensional position-sensitive detector mounted at its exit, enabling a range of target electron binding energies ε and momenta $\boldsymbol{q}$ to be measured simultaneously. This is a major advantage as it greatly improves the (e, 2e) coincidence rate.

The choice of asymmetric kinematics is very important for optimizing the energy resolution. It also provides for smaller momentum transfer ($\boldsymbol{K}$) and hence a larger coincidence cross section since the electron–electron cross section is at these energies proportional to $\boldsymbol{K}^{-4}$ where

$$\boldsymbol{K} = \boldsymbol{p}_0 - \boldsymbol{p}_f . \tag{3}$$

An additional property of the asymmetric kinematics is that the (e, 2e) measurement is sensitive to the surface of the target facing the slow-electron analyser. This arises because the escape depth of the slow electron is only about 20 Å, and hence the (e, 2e) event must

occur in the outermost layers. It is this property that makes it possible to perform these measurements of the band structure of aluminium.

Preparation of the aluminium samples was undertaken in a vacuum chamber directly adjoining the (e, 2e) spectrometer. In this preparation chamber there is the facility to prepare targets by evaporation onto a surface of a self-supporting thin film. Samples can also be characterized using the Auger electron spectrometer (cylindrical mirror analyser, Physical Electronics) located in this chamber. An annealing stage is also available. The sample preparation chamber base pressure is maintained in the very low 10^{-10} Torr range after baking out. In the main (e, 2e) spectrometer the pressure after bake-out is around 7×10^{-11} Torr. Samples can be readily transferred *in situ* between the two chambers, minimizing the possibility of surface contamination.

Sample preparation of aluminium originates with 50 Å amorphous carbon films from Arizona Carbon Foil Company. These films are sliced into $\approx$10 mm squares and floated off their glass slides into a bath of deionized water. From here a film is collected onto a molybdenum sample holder containing 1 mm diameter holes so that as many holes as possible are covered. This sample holder containing the free-standing carbon films is then transferred into the preparation chamber. The amorphous carbon film is annealed at 3 W for 10 min to remove any oxygen from the surface. The annealing also increases the conductivity of the carbon film, avoiding charging problems during the EMS experiments as is occasionally encountered with untreated films. Annealing power is achieved by bombarding the sample holder with electrons from a tungsten filament. A bias of 1 kV is applied between the filament and sample holder, resulting in a current of 3 mA on the sample. A 40 Å aluminium layer was evaporated onto the thin amorphous carbon substrate. The thickness of the evaporated layer was determined from a crystal thickness monitor. During the evaporation the pressure increased by about a factor of 100; however, after 10 minutes it had recovered back to the base pressure of 1.0×10^{-10} Torr. The sample was then immediately transferred under vacuum into the (e, 2e) spectrometer to minimize the chance of oxygen contamination.

Auger electron spectroscopy has also been performed on separate aluminium samples that were prepared in exactly the same manner. The Auger spectrum is comprised mostly of the signal from metallic aluminium LMM (70 eV); however, a small amount of oxygen KLL (510 eV) can be detected. This oxygen signal is around an order of magnitude smaller than that of aluminium. It should also be noted that the Auger spectrometer is more surface sensitive than our (e, 2e) spectrometer, and hence the chance of detecting this signal is minimal. In a separate series of experiments the aluminium films were exposed to well controlled amounts of oxygen. Significant changes to the valence band structure were not observed until the exposure was greater than 100 L (Canney *et al* [13]). With the limited surface sensitivity of the (e, 2e) spectrometer we do not expect oxygen to affect the valence band of the evaporated films in any significant way.

3. The electronic structure of aluminium

Aluminium is a face-centred cubic (FCC) metal and its associated Brillouin zone is the truncated octahedron shown in figure 2(a). The band structure of aluminium has been calculated by many groups and is well known to mimic a nearly free-electron band structure; see for example Ashcroft and Mermin [14]. In aluminium a single s–p valence band is formed from the 3s and 3p valence electrons. These valence electrons can be described using the nearly free-electron approximation.

In 1983 Levinson *et al* [15] published very detailed results on the experimental band

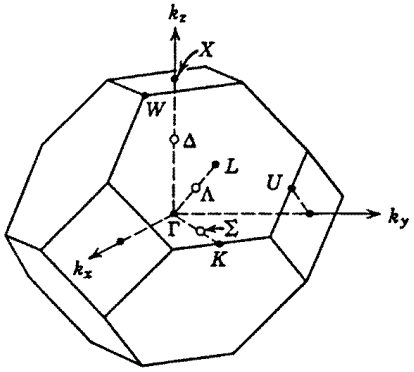

(a)

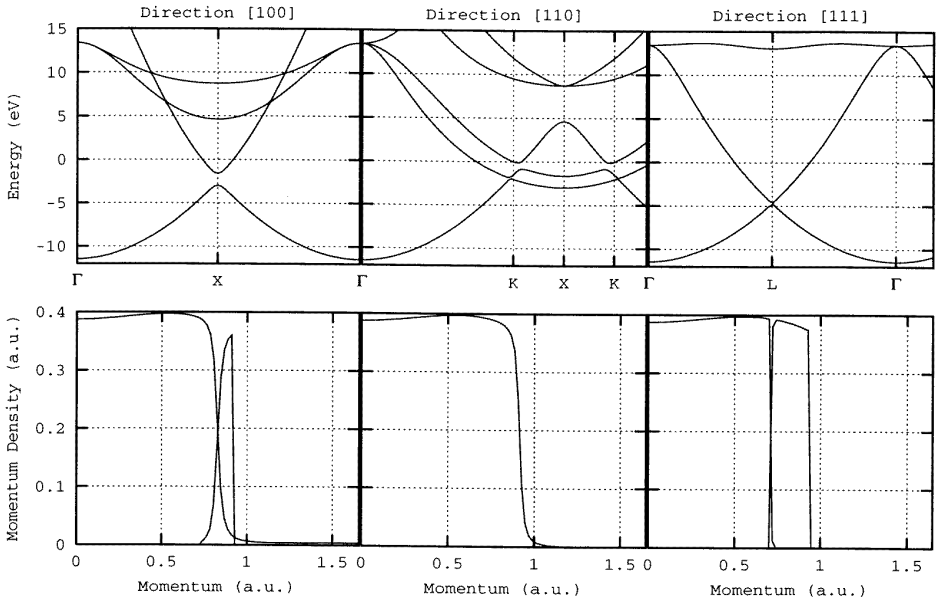

(b)

Figure 2. (a) shows the Brillouin zone of aluminium and (b) shows the energy bands and momentum densities along the Γ–X, Γ–K and Γ–L symmetry directions as determined from the LMTO calculation.

structure of aluminium in the Γ–X and X–W directions in the Brillouin zone using angle-resolved photoemission. (e, 2e) spectroscopy has the potential to measure this, plus information on the momentum densities, in a single experiment. Since the valence band structure of aluminium is widely known, we decided that it would be an ideal experiment to test our understanding of the (e, 2e) reaction on solids and to quantify these results with LMTO calculations and Monte Carlo simulations.

We used the LMTO method in the atomic sphere approximation (ASA) as described by Skriver [16]. The atomic sphere radius calculated from the experimental lattice constant

$a = 7.60$ au is given by

$$R_s = \frac{a}{2}\left(\frac{3}{2\pi}\right)^{1/3} = 2.97 \text{ au.} \tag{4}$$

The band-resolved energy-dependent electron momentum density is expressed through the Fourier transform of the one-electron wave-function ψ_{jk} obtained by the LMTO calculation:

$$\rho_j(\epsilon, \boldsymbol{q}) = (2\pi)^{-3} \sum_{G\boldsymbol{k}} n_{j\boldsymbol{k}} \left| \int \mathrm{d}^3 r \; \psi_{j\boldsymbol{k}}(\boldsymbol{r}) \mathrm{e}^{-\mathrm{i}\boldsymbol{q}\cdot\boldsymbol{r}} \right|^2 \delta_{\boldsymbol{q},\boldsymbol{k}+\boldsymbol{G}} \, \delta(\epsilon - E_j(\boldsymbol{k})) \qquad \boldsymbol{k} \in \text{1st BZ.} \tag{5}$$

Here j is the band index, and $n_{j\boldsymbol{k}}$ and $E_j(\boldsymbol{k})$ are the occupation number and energy of the corresponding one-electron state. The integration in equation (5) is carried out over the unit cell where the wave-function $\psi_{j\boldsymbol{k}}$ is normalized to unity. The reciprocal-lattice vector $\boldsymbol{G}$ translates the momentum $\boldsymbol{q}$ to the first Brillouin zone (BZ). The energy-dependent electron momentum density is normalized over energy and momentum space to the number of valence electrons per unit cell per spin:

$$2 \sum_j \int \mathrm{d}\epsilon \; \mathrm{d}\boldsymbol{q} \; \rho_j(\epsilon, \boldsymbol{q}) = N_e. \tag{6}$$

The band-resolved energy-independent electron momentum density $\rho_j(\boldsymbol{q})$ can be obtained from an expression similar to equation (5) in which the δ-function of the energy is omitted.

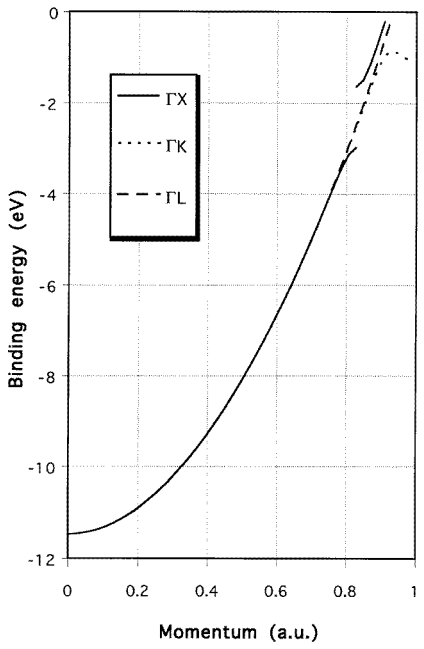

Figure 3. The dominant contribution of the energy bands for the three symmetry directions (Γ–X, Γ–K and Γ–L) as determined from the LMTO calculation plotted between 0 and 1 atomic units. The band gap in the Γ–X direction becomes filled by the contributions from the other symmetry directions when the energy bands are spherically averaged.

The results of the LMTO calculation in three major high-symmetry directions are summarized in figure 2(b) where we plot the energy bands $E_j(\boldsymbol{q}-\boldsymbol{G})$ and momentum densities $\rho_j(\boldsymbol{q})$. Here $\boldsymbol{q} = q\boldsymbol{e}$ where $\boldsymbol{e}$ is the unit vector in the given direction and q is a scalar. In (e, 2e) spectroscopy, real momentum is measured, not crystal momentum. It is thus important to know in which Brillouin zone the bands are occupied. This is also indicated in figure 2(b). Our preparation technique for aluminium, i.e. evaporation onto an amorphous carbon substrate, gives a polycrystalline aluminium sample. The implication of this is that what is then measured in an (e, 2e) experiment is a spherical average. The dispersion of the Γ–X, Γ–K and Γ–L directions can be seen as extreme cases. To further illustrate this point we have plotted the dominant electron band contribution for each of these three directions in figure 3. The band gap in the Γ–X direction is a result of the free-electron degenerate states being split at the Brillouin zone boundary due to the weak periodic potential of the crystal. When all three directions are overlaid on each other this gap is filled from contributions from the other two crystal directions. Hence in our measurement of polycrystalline aluminium we will not be able to measure the width of this band gap. This is the only piece of information not measurable with a polycrystalline sample. This disadvantage is clearly outweighed by the much simpler sample preparation of polycrystalline aluminium as compared with monocrystal aluminium. Moreover, because the spherically averaged energy–momentum density $\rho = (|\phi(\varepsilon, \boldsymbol{q})|^2)$ is now only dependent on $|\boldsymbol{q}|$ and ε, all information is contained in a plot of ρ against two variables ($|\boldsymbol{q}|$ and ε) rather than four (q_x, q_y, q_z and ε) which simplifies the interpretation greatly. This is the first EMS experiment that gives detailed information on the dispersive nature of the valence band of aluminium *and* the densities of the electrons in the band.

4. A comparison with photoemission spectroscopy

Let us pause briefly to make a few remarks about some differences between an angle-resolved photoemission experiment on a free-electron solid and an EMS experiment. First consider a true free-electron gas, i.e. a number of electrons in a vacuum. One could readily study (at least in principle) such a system using the EMS technique. Of course for such a measurement there would be a simple relation between the momentum and energy determined (i.e. $E = p^2/2m$). A system of this type would be impossible to study using photoemission since a free electron cannot absorb a photon without violating the laws of energy and momentum conservation.

Now consider a material with electrons that behave almost as in a free-electron gas. In a nearly free-electron metal the motion of the electrons is hardly affected by the weak periodic potential of the lattice. Thus the spectral momentum density is almost independent of the orientation of the lattice. Hence an EMS measurement is almost independent of crystal orientation, and so even a polycrystalline sample will clearly show the features of a free-electron metal.

The situation is somewhat different for photoemission. Momentum conservation is a consequence of the complete translation symmetry of space, preventing a photon from being absorbed by a true free electron. The small lattice potential makes absorption of photons possible. This potential is only invariant for translation over a lattice vector, and hence momentum conservation is replaced by conservation of crystal momentum. Thus one can absorb a photon provided that the initial and final states have the same crystal momentum. To visualize these transitions one plots the band structure in the reduced-zone scheme and photon absorption is allowed for a vertical transition between bands plotted in this representation.

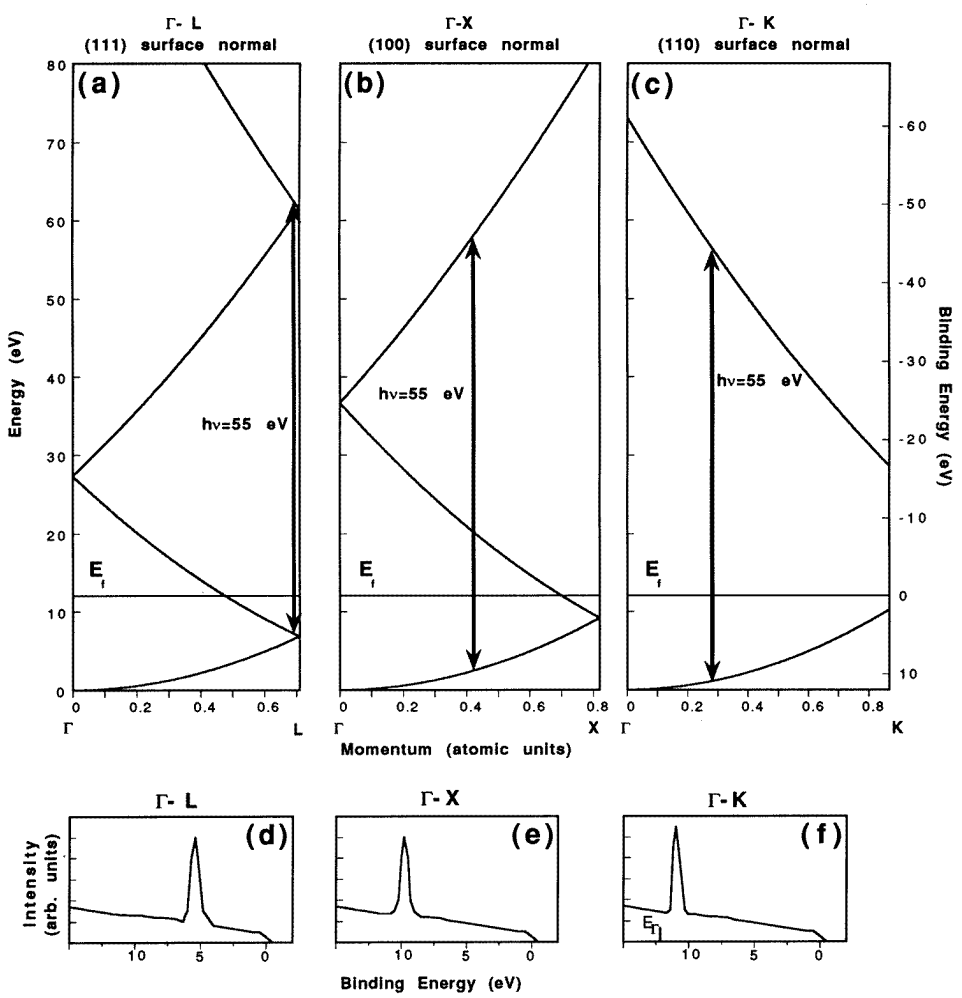

Figure 4. The band structure of a FCC free-electron metal plotted in the reduced-zone scheme in the (111), (100) and (110) directions ((a)–(c)). The Fermi level (E_F) was chosen to be at 12 eV relative to the bottom of the band. Only bands for which the electron momentum would be parallel to the surface normal are shown. Possible transitions for absorption of a photon of 55 eV are shown. In a normal-emission ARPES experiment one would see spectra as shown schematically in (d)–(f) for crystals with their surface normal along these respective directions. Also shown in (f) is the position of the bottom of the band (E_Γ). Even for a free-electron metal the observed spectra depend on crystal orientation, and it is thus impossible to infer dispersion relations from a true polycrystalline sample.

In the conceptually simplest forms of photoemission one measures the electrons emitted perpendicular to the surface. In this way the potential step at the surface does not affect the direction of propagation of the electrons. In figure 4 we show the allowed transition for a FCC free-electron metal similar to aluminium. Due to the peculiar shape of the Brillouin zone, the distance from the centre (Γ) to the boundary depends on the direction. Thus, depending on the surface orientation, we obtain in the reduced-zone scheme, *even* for a perfect free-electron gas, a completely different band-structure diagram for different sample

orientations (perfect as far as dispersion is concerned; still enough interaction with the lattice to allow photoabsorption). Thus for a photon energy of say 55 eV, we get peaks at different binding energies for normal-emission experiments of crystals with (100), (110) or (111) surfaces (figure 4, lower half). For a polycrystalline sample that consists of crystallites with only these three orientations, the spectrum would be the sum of these three spectra. Clearly, a true polycrystalline sample with entirely random orientations of the crystallites would give an even more smeared out result. It then becomes impossible to infer the dispersion of the band by mapping peak positions as a function of photon energy, as is readily done for single crystals.

The determination of the electronic structure is completely decoupled from the crystal structure in an EMS experiment. This is a very nice feature of (e, 2e) spectroscopy. It also makes it possible to measure 'dispersion' relations for not only polycrystalline materials, but even amorphous materials; see for example [17–19].

5. Monte Carlo simulations

The results of the previously described LMTO calculations would describe the experimental data if all (e, 2e) events were 'clean', i.e. further elastic or inelastic scattering of either the incoming or both outgoing electrons does not occur. However, only a very small proportion of (e, 2e) events occur without multiple scattering, even for thin films ($\leqslant$100 Å) and high electron energies (several keV). In order to quantitatively compare our measured dispersion relations and intensities with the theory, we need to use Monte Carlo simulations. The Monte Carlo procedure gives an impression of the rate at which certain momentum-transfer (elastic scattering) and energy-loss (inelastic scattering) combinations occur and how this in turn affects our measured spectra. For a detailed description of the Monte Carlo procedure as previously applied to (e, 2e) spectroscopy of solids, see Vos and Bottema [20]. In the remainder of this section a summary of the procedure is given, together with a discussion on some extensions of the model not described by Vos and Bottema [20].

A description of the (e, 2e) process can be made in close analogy to the three-step model proposed originally by Berglund and Spicer [21] for photoemission experiments. This model looks at particle excitation, propagation and escape from the crystal being measured. The first and third steps in this process are well defined for an (e, 2e) event on solids. It is the second step, propagation through the sample, that we need to simulate using the Monte Carlo procedure. This simulation needs to be performed on the incoming and both outgoing electrons that constitute the (e, 2e) event.

The first part of the Monte Carlo procedure is to read in the energy-resolved momentum densities determined from the LMTO calculation. The extended Monte Carlo procedure allows for the simulation of two layers of different film types and different thicknesses. For the aluminium sample, energy-resolved momentum densities for both amorphous carbon (substrate) and aluminium (evaporated layer) are read in from a file. The simulation then involves the inclusion of both elastic and inelastic scattering events for any of the three electrons throughout both layers. If an inelastic scattering event occurs, the measured binding energy will be shifted to higher binding energies, i.e. there will be energy loss. For elastic scattering events there can be momentum transferred in either of the three momentum directions q_x, q_y or q_z. These particular shifts are illustrated in figure 5 for the case of a free-electron solid.

The depth t at which an (e, 2e) event occurs is determined in the calculation by the first number produced by a random-number generator ($t = \mathrm{Rand}_1\, T$). Here T is the thickness of the film being considered. We then need to simulate each of the three trajectories

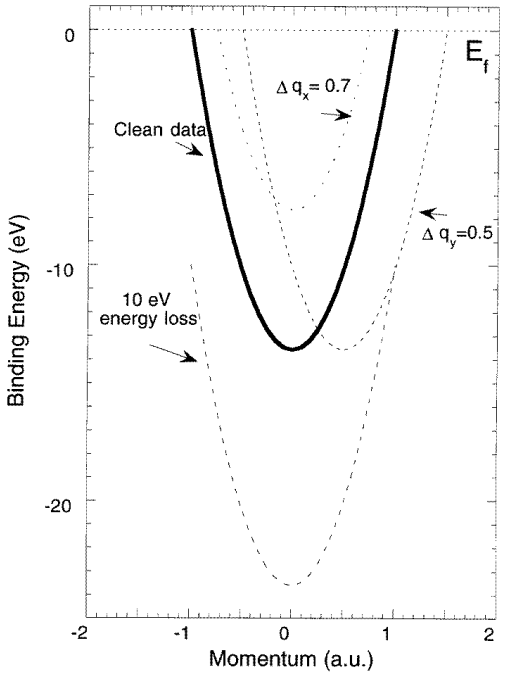

Figure 5. Possible effects of multiple scattering on the free-electron dispersion. The events with no additional multiple scattering in any of the three continuum electron trajectories involved will contribute to the intensity along the dark line. Those electrons for which only inelastic multiple scattering occurs—of say 10 eV—will add intensity to the lower dotted line, i.e. there will be energy loss. Those electrons which experience elastic scattering in the y-direction will contribute to the intensity along the curve shifted by 0.5 au. If scattering occurs causing a momentum shift along the x-direction (or similarly the z-direction) (but with $\Delta q_y = 0$) it will cause intensity along a curve shifted upwards relative to the clean data. The x-, y- and z-coordinate frame is defined in figure 1.

for electrons with energy E_0, E_f and E_s and trajectory length t_0, t_f and t_s. The procedure followed is identical for each of the three electrons involved. For elastic scattering the cross sections for both carbon and aluminium are input into the program. These cross sections are calculated in the Born approximation from Hartree–Fock wave-functions of the free atom. For inelastic scattering only bulk plasmon excitations are considered. It is assumed that the plasmon distribution is Gaussian, centred at some mean plasmon energy. Both the energy of the plasmon and the width of the Gaussian (experimentally determined) are read from files for carbon and aluminium respectively. From these input parameters the elastic and inelastic mean free paths for each of the three electrons involved are determined. In the simulation the probabilities of distances between subsequent elastic and inelastic scattering events vary as a Poisson distribution characterized by the mean free path. Using Monte Carlo methods the occurrence of elastic and inelastic scattering combinations is calculated for each of the three trajectories using these Poisson distributions. If the distance for elastic or inelastic scattering obtained from the distribution is smaller than the depth t, a contribution is made to the energy-resolved momentum density. For elastic scattering the azimuthal angle, and hence momentum transfer, of the scattering event is obtained. For inelastic scattering the energy of the particle is decreased by the amount of the plasmon energy. All three

trajectories are simulated for both elastic and inelastic scattering events through both layers of the film. After this all energy losses (inelastic scattering) and momentum transfers (elastic scattering) are added and an energy-resolved momentum density for the sample is obtained.

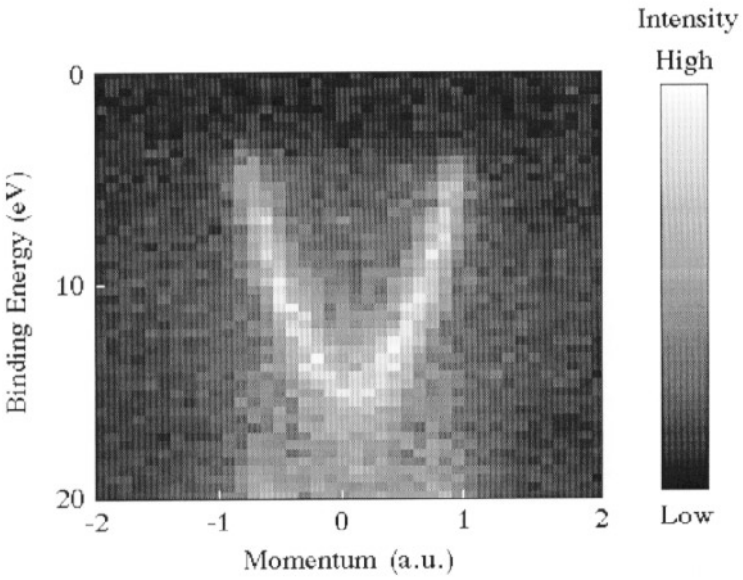

Figure 6. An experimentally measured energy-resolved momentum density plot for the polycrystalline aluminium sample. The intensity is given by a linear grey-scale; the lighter the colour, the higher the intensity. Binding energy is relative to the vacuum level. The energy–momentum pixels have $\Delta\varepsilon = 0.4$ eV and $\Delta q_y = 0.1$ au.

6. Valence band results and discussion

An (e, 2e) measurement was made on the valence band of aluminium with the experimental settings as described in section 2. The sample was measured for a period of two days with a true coincidence count rate of about 100 counts min^{-1}. The energy-resolved momentum density plot for the aluminium valence band raw data is shown in figure 6. In this plot the dispersion curve for the valence band of aluminium clearly stands out above the background. The densities are represented as a linear grey-scale image, with the lightest scale corresponding to the highest intensity. In this plot the pixel size is 0.4 eV in energy and 0.1 au in momentum. The dispersion curve looks very similar to a free-electron band as was expected for metallic aluminium. The parabola extends from 4 eV binding energy at the top, down to 16 eV at the bottom. It should be noted that our experimental binding energies are referenced to the vacuum level not the Fermi level. The Fermi level corresponds to 4.0 ± 0.5 eV binding energy in the experiment. Our measured bandwidth of 12 eV is close to that calculated for aluminium using the LMTO method (11.5 eV). The band is occupied in momentum space between $\simeq -1.0$ and 1.0 atomic units.

For a quantitative study—that is, the determination of the energy–momentum position of the electrons and the relative intensities—a more thorough analysis is required. For this purpose we have constructed a series of momentum profiles by taking slices through the

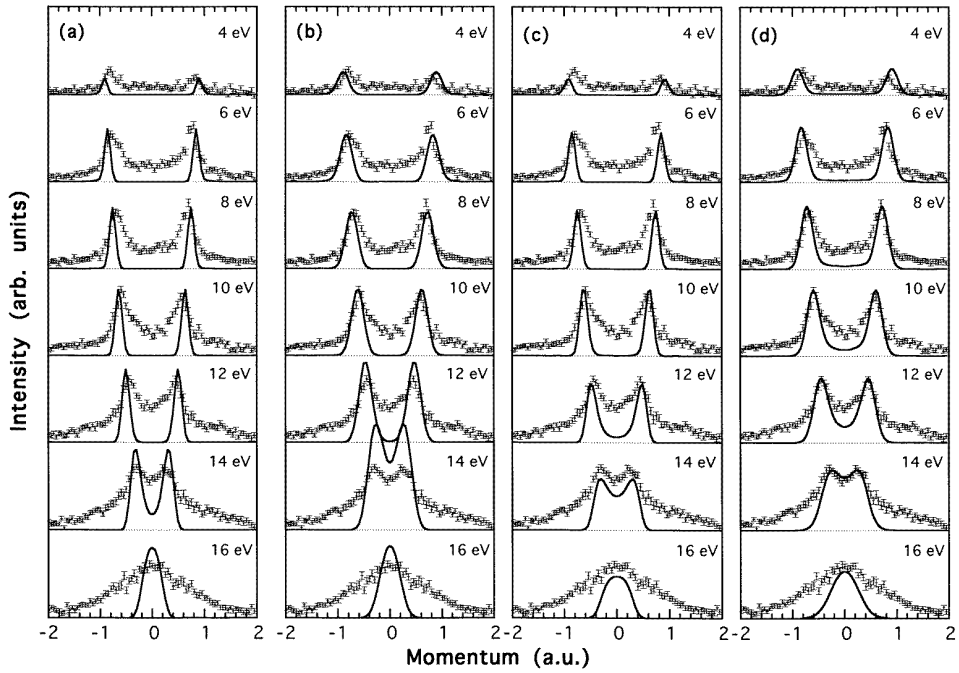

Figure 7. The momentum profiles of the measured aluminium sample for a series of energies are shown with error bars in each of the four panels. Also shown are the LMTO calculations (solid lines) for (a) convolution with 1 eV energy resolution, and (b) convolution with 2 eV energy resolution and 0.1 atomic unit momentum resolution. In (c) the calculation has been fitted with a Gaussian for the experimental resolution (1 eV FWHM) and one which represents a curve for the energy broadening due to lifetime effects as measured by Levinson *et al* [15]. In (d) we show the LMTO calculations of (c) plus a convolution for the momentum resolution of 0.1 au.

valence band region (the width of the slices is 1 eV) with the centre of those slices being at the binding energy indicated. The experimental momentum profiles are shown (with error bars) in figure 7. From these plots one can see two distinct peaks at the top of the band (4 eV) which are symmetric around zero momentum. As the energy increases these peaks disperse inwards, i.e. towards zero momentum, finally forming one peak centred at zero momentum at the bottom of the band (16 eV). For a detailed analysis we need to compare these experimental momentum profiles with results obtained from LMTO calculations on the valence band of aluminium.

The momentum profiles of the LMTO calculation are represented by the solid lines in figure 7(a). These calculations are made with reference to the Fermi level; hence the calculation has been shifted by 4 eV to account for the fact that the Fermi level of the spectrometer was found to be at 4 eV. This calculation has been convoluted with an energy resolution of 1.0 eV to match the measured energy resolution of the (e, 2e) experiment [9]. For a first attempt the agreement between experiment and theory is already very good; however, there are some discrepancies. For the position of the peaks the calculation agrees closely with the experiment; however, it predicts the peak position at slightly higher momentum near the top of the band than is observed in the experiment. The discrepancy is, even at the Fermi level where it is largest, only about 0.05 au. This value is smaller than

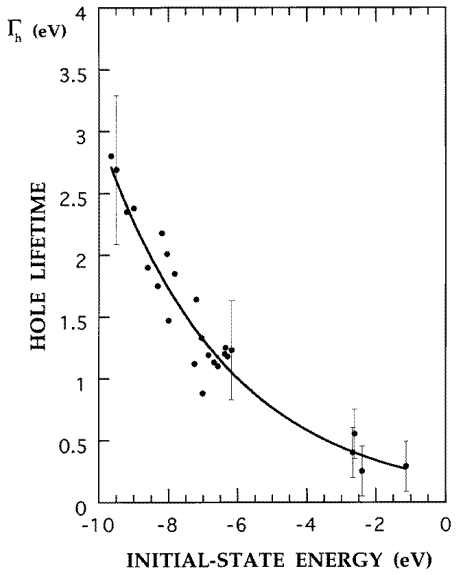

Figure 8. Hole lifetime widths as deduced from angle-resolved photoemission by Levinson *et al* [15] plotted against the energy below the Fermi level. Also shown is our curve of best fit used in the convolution for energy broadening due to lifetime effects in the LMTO calculation.

our estimated momentum resolution. The resolution refers to the minimum full width at half-maximum (FWHM) of a momentum peak that we can expect to measure. Clearly we can determine the position of the peaks at least three times more accurately than the FWHM of the peak. As far as intensities are concerned we have normalized the LMTO calculation with the experiment at 10 eV. The agreement of intensity of the peaks themselves is very good except near the bottom of the band. At 14 eV and 16 eV the calculations predict higher peak intensity than is measured in the experiment. The glaring discrepancy between experiment and theory is the excess intensity in between the peaks and the broadening of the peaks seen in the measurement. Also outside of the peaks, i.e. at higher momentum, the measurement shows non-zero intensity. These discrepancies in intensity are common to all samples measured thus far and we aim to resolve this with our discussion of the Monte Carlo simulations. It should also be noted that the width of the peaks is clearly underestimated even when including the known experimental energy resolution in the calculation.

The experiment also has a finite momentum resolution which is determined by the angular resolution of each of the three electron beams and the resolution of both of the electron analysers. It is complicated to get an estimate of the momentum resolution since $\boldsymbol{q}$ needs to be treated as a vector, i.e. there is a different contribution for each of the three directions. Unlike energy resolution, where we could measure experimentally a peak which is known to be sharp (the C 1s core level), it is difficult to obtain an estimate of the momentum resolution under experimental conditions. However, for consistency we need to also convolute the LMTO calculations with a Gaussian that represents the finite momentum resolution as well as one for the energy resolution of the experiment. An upper estimate of the spherically averaged momentum resolution of 0.15 au was given by Storer *et al* [8] based on measurements of the argon 3p momentum resolution. The collimation of the incident beam has since been improved so an estimate of the momentum resolution of 0.1 au was

made. In figure 7(b) we have plotted the results of the LMTO calculation convoluted with 2.0 eV energy resolution and 0.1 au momentum resolution. The experimental results are also shown in this plot for comparison. The calculated peak widths are again if anything too narrow, and near the Fermi level the predicted peak position is still 0.05 atomic units further from zero momentum than is seen in the experiment. In addition, as a result of including the momentum convolution, the intensity towards the bottom of the band has been exaggerated from the overlap of the fitted Gaussians. In a search for fully quantitative agreement we require some extra information to be included in our theoretical calculations.

Up until this point no consideration has been given to the effect of the hole lifetimes on our (e, 2e) results. That is we have not considered the energy broadening caused by the finite lifetime of the hole resulting from the ejection of one electron. Levinson *et al* [15] measured the hole lifetimes in their angle-resolved photoemission experiments on aluminium. A reproduction of their plotted results is given in figure 8. From this figure it is obvious that the effect of lifetime broadening cannot be omitted, particularly near the bottom of the band. These results show that at the top of the band the lifetime effects can be neglected. The reason for this is that after removing an electron from the top of the band (leaving a hole) there are no higher occupied levels which an electron can vacate to fill this hole, leading to a long hole lifetime, and the resolution of the system is then only the experimental resolution of the apparatus. However, if an electron is knocked out with a higher binding energy, i.e. towards the bottom of the band, the hole that is created can readily be filled by an electron from states of lower binding energy. The electron–hole contribution at the bottom of the band to the energy width reaches 3 eV and these effects need to be included in our calculations. To account for lifetime broadening effects we fitted the LMTO calculation with two curves. The first was a Gaussian of width 1 eV corresponding to the instrumental energy resolution of our spectrometer. We also convoluted the calculation with a Lorentzian representing the best fit to the experimentally determined points of Levinson *et al* [15]. The momentum profiles for this LMTO calculation are shown together with the experimental results in figure 7(c). There are obvious improvements to the agreement obtained. The intensity of the peaks agrees very well throughout the band. At the bottom of the band the intensity obtained from the calculation is now actually slightly lower than that of the experiment. This calculation does not however include the finite momentum resolution of the experiment which we have shown increases the intensity at the bottom of the band. Once again the calculation does not predict the measured intensities between the peaks and at momentum outside the peaks.

The momentum profiles obtained if we include the lifetime widths, experimental energy resolution (1eV) and the finite momentum resolution (0.1 au) in the LMTO calculation are shown in figure 7(d) together with the experimentally determined profiles. The agreement between the experiment and the LMTO calculation is now excellent. The intensities of the peaks and their widths compare very well indeed. There is still the slight discrepancy between the positions of the peaks near the Fermi level. Once again the peaks are calculated to be around 0.05 atomic units towards higher momentum than what is measured.

Having achieved the best possible agreement between the experimental results and LMTO calculations, we investigated the effects of elastic and inelastic scattering on the measured energy-resolved momentum density using the Monte Carlo procedure described in section 5. In figure 9 we have plotted linear grey-scale energy–momentum densities of the experimental results, the LMTO calculation including all of the above effects (figure 6(d)) and a Monte Carlo simulation based on the LMTO calculation. A comparison of the measurement and LMTO calculation has already been discussed. The binding energy scale of this plot ranges from 0 to 50 eV, so a discussion of the multiple-scattering

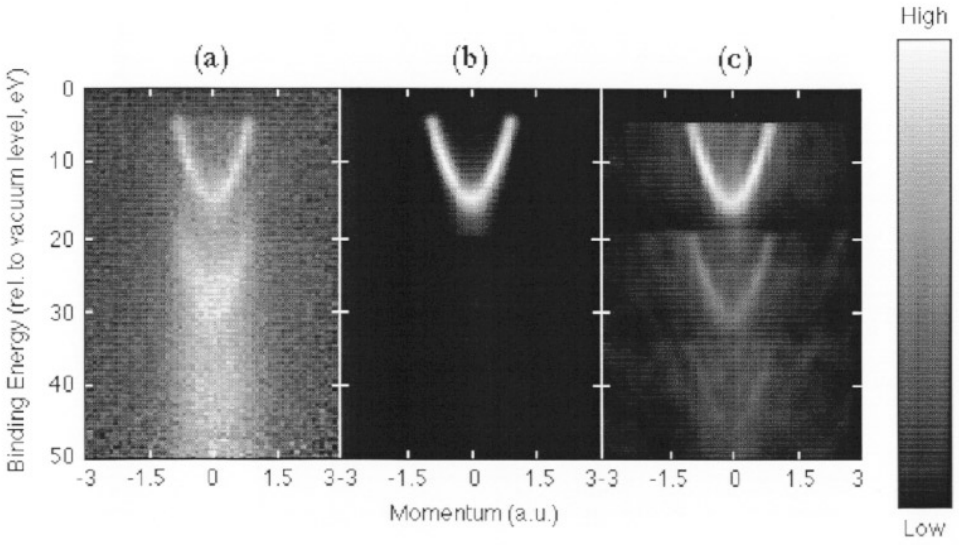

Figure 9. The energy-resolved momentum density for the (e, 2e) measurement of aluminium (a), and as calculated using the LMTO method convoluted with Gaussians representing the finite experimental energy and momentum resolutions and the energy broadening due to finite-lifetime effects [15] (b), and as simulated using the Monte Carlo procedure taking the LMTO calculated momentum density as input (c).

events can also be given. Qualitative improvement of the agreement between theory and experiment is obtained after inclusion of the Monte Carlo simulation. The valence band of the measurement is simulated very well using the Monte Carlo procedure. There is extra intensity inside and outside the valence band from the Monte Carlo simulation that is not seen as clearly in the LMTO calculation. In the (e, 2e) measurement the plasmon dispersion of aluminium can clearly be seen. The plasmon dispersion is a replica of the aluminium valence band shifted to 15 eV lower binding energy, i.e. inelastic scattering resulting in energy loss. The Monte Carlo simulation also predicts this plasmon dispersion; however, the intensity of the plasmon distribution is not as high as in the measurement. Also the plasmon distribution from the experiment appears to be 'filled in' and this is not seen in the Monte Carlo simulation. The Monte Carlo simulation does predict a plasmon distribution of double excitation, i.e. 30 eV energy loss. This second plasmon distribution cannot be conclusively resolved in the measurement.

For a quantitative study of the final result of the (e, 2e) measurement, the LMTO calculation and Monte Carlo simulation, further analysis is required. To do this we have plotted momentum profiles at 1 eV intervals for the measurement (error bars), LMTO calculation (solid line) and Monte Carlo simulation (dashed line) in figure 10. The discrepancies between the measurement and LMTO calculation have already been discussed. It is clear that the Monte Carlo simulation has significantly increased the intensity between the two peaks, i.e. where the LMTO calculation predicted zero intensity. The mechanism responsible for this is elastic scattering. Up to 12 eV the agreement is very good. Above 12 eV the peak intensities themselves are in very good agreement although the measurement shows intensity at higher momentum that is not predicted in either of the theoretical models. This excess intensity is most likely a result of inelastic processes that are not accounted for in the Monte Carlo procedure. These processes include surface plasmon excitation and the

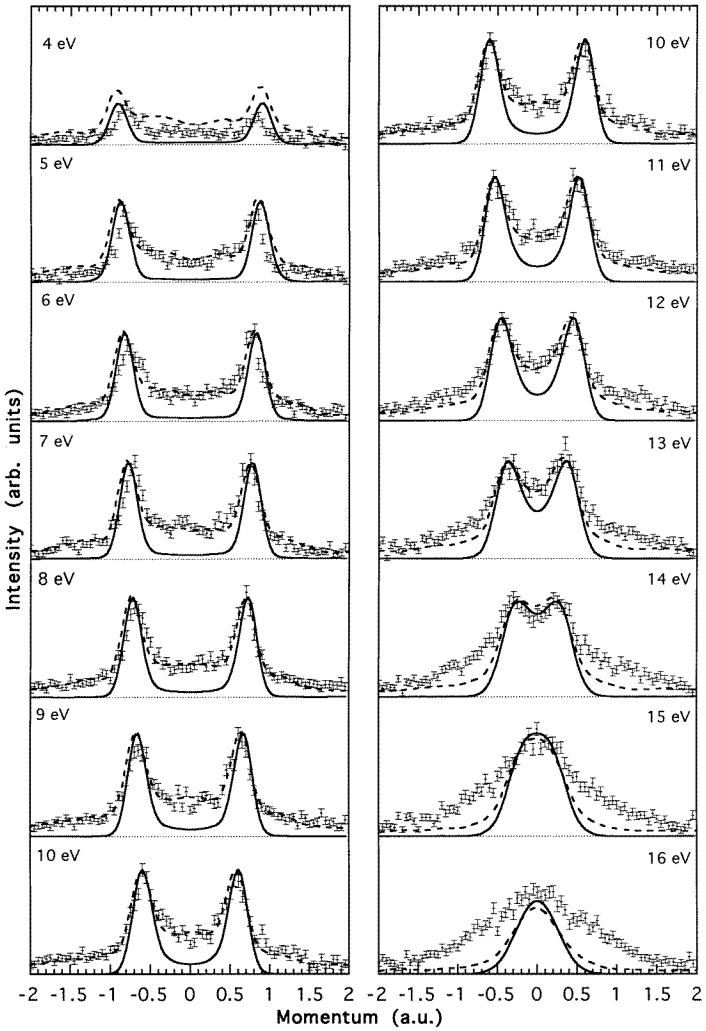

Figure 10. The measured momentum profiles in 1 eV bins for aluminium at a series of energies are shown with the error bars. Also shown are the momentum profiles for the full LMTO calculation (solid lines) of figure 6(d) and the profiles obtained from the Monte Carlo simulations (dashed lines).

effects of momentum transfer during plasmon excitation and single-electron excitations.

Binding energy spectra at 0.1 au intervals are shown in figure 11. Due to symmetry about zero momentum, the positive and negative momentum components have been combined in this figure. At the bottom of the band ($\boldsymbol{q} \approx 0$) in the experimental plot there is a peak at 15 eV in the valence band and another broad peak centred at around 29 eV resulting from plasmon excitation. The valence band and plasmon peak clearly disperse to lower binding energy as the momentum increases. This dispersion in the valence band and also the relative intensities are closely predicted in the LMTO calculation. Obviously the dispersion of the plasmon is not seen in the LMTO calculation as inelastic scattering events are not accounted for. The Monte Carlo simulation does however show the plasmon dispersion;

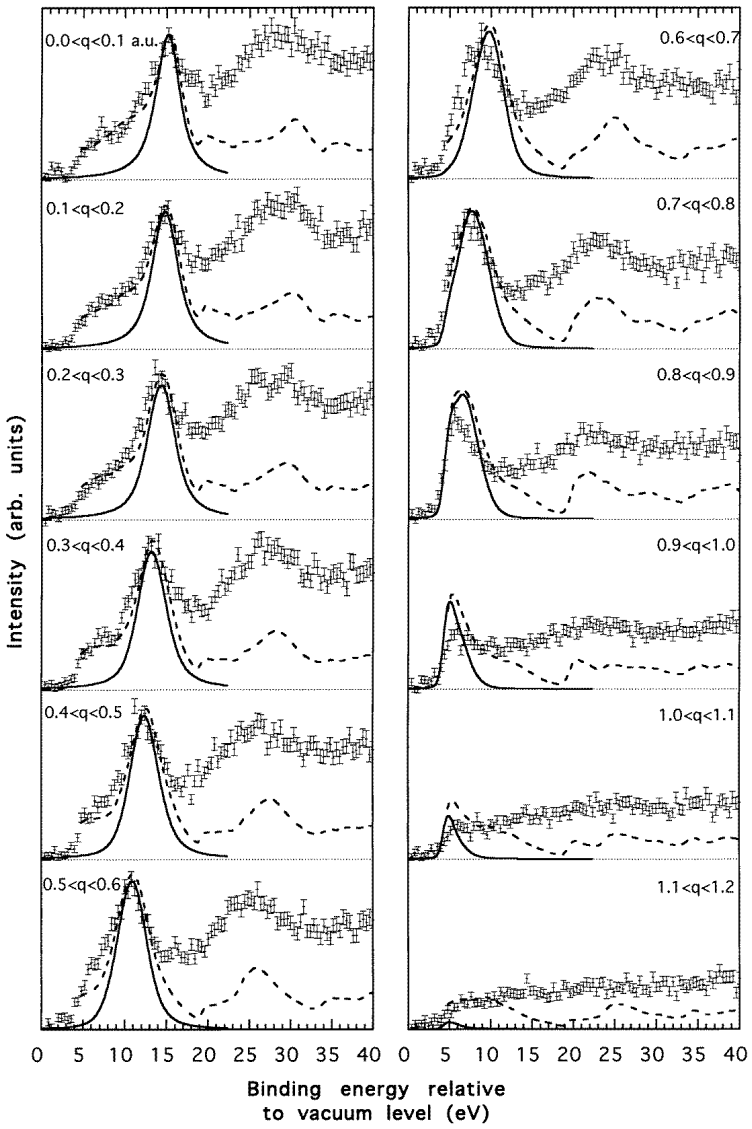

Figure 11. The measured energy profiles for aluminium at a series of momenta are shown with the error bars. Also shown are the energy profiles for the full LMTO calculation (solid lines) and the profiles obtained from the Monte Carlo simulations (dashed lines).

the position of the plasmon for each of the momenta compares well with the measurement. However, the predicted plasmon intensity from the simulation is only about half that from the measurement. This discrepancy probably arises from inelastic processes not allowed for in the Monte Carlo simulation.

The discrepancy between theory and experiment of 0.05 au in peak position at the top of the valence band in the momentum profiles deserves some discussion. The kinematics of our spectrometer allows momentum to be measured only along the y-direction; see figure 1. What is plotted in the momentum profiles is then q_y against intensity as a function of binding

energy. The experimental kinematics was chosen so that the slice of y-momentum measured goes through the $\boldsymbol{q} = 0$ point (i.e. $q_x = q_z = 0$ when $q_y = 0$). A misalignment could lead to an offset of non-zero q_x or q_z, as a result of which the slice would no longer go through $\boldsymbol{q} = 0$. This would lead to a narrowing of the measured momentum profile at the Fermi level. It would require an offset of about 0.3 au to explain the measured discrepancy of 0.05 au in the position of the peaks. However, such an offset would also affect the position of the bottom of the band, since the measured momentum slice would then not go through the Γ point. Indeed, the bottom of the band would have to be about 1.5 eV lower than that measured, i.e. the bandwidth would have to be about 13.5 eV instead of the currently measured 12 eV, which is in excellent agreement with the calculated 11.5 eV. In the band-structure measurements of Levinson *et al* [15] an occupied bandwidth of only 10.6 eV was reported. This is significantly smaller than the present measured and calculated bandwidths. Although we do not understand this discrepancy it could similarly be explained if the angle-resolved photoemission studies have a momentum offset in the non-measured momentum directions. Further comparisons between EMS and ARPES band structures should be most interesting, and we are currently pursuing this course with measurements on an oriented single crystal of graphite. We are also pursuing the question of a possible momentum offset in our measurements with the graphite sample where all momentum directions are clearly defined and the π-band has a null in the Γ–K and Γ–M plane. We would also like to stress the fact that it is only possible to observe these minor discrepancies because of the large improvements made to the (e, 2e) experiments on solids over the last few years.

7. Conclusion

Electron momentum spectroscopy ((e, 2e) spectroscopy) has been used to measure the energy-resolved momentum densities of a polycrystalline aluminium sample. The dispersion curve obtained from the measurement very closely resembles the classic free-electron band seen in textbooks. The measurement also shows that the valence band is occupied with approximately equal intensity throughout. A detailed comparison of the experimental results is made with several LMTO calculations, including convolutions for the energy and momentum resolutions of the spectrometer. In addition, in order to obtain very good agreement with the measurements, it was essential to include the energy broadening due to finite-hole-lifetime effects. This is the first time that hole lifetimes have been considered for (e, 2e) studies on solid-state systems. The present (e, 2e) measurements confirm the hole lifetimes obtained by Levinson *et al* [15] in their photoemission studies. The experimental results are also compared to Monte Carlo simulations which include elastic and inelastic scattering events other than the (e, 2e) event itself. These additional scattering events are not considered in the LMTO calculations. The agreement obtained between the experimental results and theoretical calculations is excellent when the experimental energy and momentum resolutions, the finite hole lifetimes, and inelastic and elastic scattering of the continuum electrons are considered. This study has improved our understanding of the (e, 2e) process in solids considerably and has provided us with a very direct 'image' of the electronic structure of aluminium in momentum space. The measured and calculated bandwidth of about 12 eV is somewhat larger than the 10.6 eV obtained in the ARPES measurements of Levinson *et al* [15]. The reason for this discrepancy is at present not understood, but we intend to pursue this question via comparisons for other simple targets such as graphite. Similarly the LMTO calculations give a slightly wider band at the Fermi level than observed in the current measurements. Possible explanations of this affect are also being explored with our graphite measurements.

Acknowledgments

The authors would like to thank the staff of the Electronic Structure of Materials Centre for their invaluable contributions to these (e, 2e) experiments. The Electronic Structure of Materials Centre is supported by a grant of the Australian Research Council.

References

[1] McCarthy I E and Weigold E 1988 *Rep. Prog. Phys.* **51** 299
[2] McCarthy I E and Weigold E 1991 *Rep. Prog. Phys.* **54** 789
[3] Lohmann B and Weigold E 1981 *Phys. Lett.* **86A** 139
[4] Amaldi U Jr, Egidi A, Marconero R and Pizzella G 1969 *Rev. Sci. Instrum.* **40** 1001
[5] Camilloni R, Guardini-Guidoni A, Tiribelli R and Stefani G 1972 *Phys. Rev. Lett.* **29** 618
[6] Persiantseva N M, Krasil'nikova N A and Neudachin V G 1979 *Sov. Phys.–JETP* **49** 530
[7] Ritter A L, Dennison J R and Jones R 1984 *Phys. Rev. Lett.* **53** 2054
[8] Storer P, Caprari R S, Clark S A C, Vos M and Weigold E 1994 *Rev. Sci. Instrum.* **65** 2214
[9] Canney S A, Brunger M J, McCarthy I E, Storer P J, Utteridge S, Vos M and Weigold E 1997 *J. Electron. Spectrosc. Relat. Phenom.* at press
[10] Courths R and Hufner S 1984 *Phys. Rep.* **112** 53
[11] Cooper M J 1985 *Rep. Prog. Phys.* **48** 415
[12] Williams J F and Hayes P A 1990 *Aust. J. Phys* **43** 465
[13] Canney S A, Vos M, Kheifets A S, Guo X, McCarthy I E and Weigold E 1997 *Surf. Sci.* submitted
[14] Ashcroft N W and Mermin N D 1976 *Solid State Physics* (New York: Holt, Rinehart and Winston)
[15] Levinson H J, Greuter F and Plummer E W 1983 *Phys. Rev.* B **27** 727
[16] Skriver H L 1984 *The LMTO Method* (Berlin: Springer)
[17] Vos M, Storer P, Cai Y Q, Kheifets A S, McCarthy I E and Weigold E 1995 *J. Phys.: Condens. Matter* **7** 279
[18] Vos M, Storer P J, Cai Y Q, McCarthy I E and Weigold E 1995 *Phys. Rev.* B **51** 1866
[19] Storer P, Cai Y Q, Canney S A, Clark S A C, Kheifets A S, McCarthy I E, Utteridge S, Vos M and Weigold E 1995 *J. Phys. D: Appl. Phys.* **28** 2340
[20] Vos M and Bottema M 1996 *Phys. Rev.* B **54** 5946
[21] Berglund C N and Spicer W E 1964 *Phys. Rev.* A **136** 1030